Check for updates

Role of a Pdlim5:PalmD complex in directing dendrite morphology

Yogesh Srivastava[1]*, Maxsam Donta[1,2], Lydia L. Mireles[3], Adriana Paulucci-Holthauzen[1], M. Neal Waxham[3,4]* and Pierre D. McCrea[1,2,4]*

[1]Department of Genetics, University of Texas MD Anderson Cancer Center, Houston, TX, United States, [2]Program in Genetics and Epigenetics, University of Texas MD Anderson Cancer Center UT Health GSBS, Houston, TX, United States, [3]Department of Neurobiology and Anatomy, UTHealth, Houston, TX, United States, [4]Program in Neuroscience, University of Texas MD Anderson Cancer Center UT Health GSBS, Houston, TX, United States

Neuronal connectivity is regulated during normal brain development with the arrangement of spines and synapses being dependent on the morphology of dendrites. Further, in multiple neurodevelopmental and aging disorders, disruptions of dendrite formation or shaping is associated with atypical neuronal connectivity. We showed previously that Pdlim5 binds delta-catenin and promotes dendrite branching. We report here that Pdlim5 interacts with PalmD, a protein previously suggested by others to interact with the cytoskeleton (e.g., *via* adducin/spectrin) and to regulate membrane shaping. Functionally, the knockdown of PalmD or Pdlim5 in rat primary hippocampal neurons dramatically reduces branching and conversely, PalmD exogenous expression promotes dendrite branching as does Pdlim5. Further, we show that each proteins' effects are dependent on the presence of the other. In summary, using primary rat hippocampal neurons we reveal the contributions of a novel Pdlim5:PalmD protein complex, composed of functionally inter-dependent components responsible for shaping neuronal dendrites.

KEYWORDS

neuron, dendrite, shape, morphology, cytoskeleton, catenin

Introduction

The shaping of dendrites enables the formation of elaborate dendritic arbors required in constructing neuronal networks (Lanoue and Cooper, 2019; Lefebvre, 2021). Further, in multiple pathological contexts, the gross morphology of dendrites is altered in ways that degrade nervous system functions. Such losses come about since neuronal activity, signaling, and plasticity each require organized synaptic connections that are dependent upon the morphology of dendrites.

Constituting a gap in knowledge, less is known about the mechanisms regulating dendritic branching or lengthening relative to the wealth of studies addressing axon trajectories (Bodakuntla et al., 2021; Zang et al., 2021), or the formation of dendritic

spines or pre- or postsynaptic densities (Runge et al., 2020; Ma and Zuo, 2022). In the context of neuronal dendritic branching, we recently reported that Pdlim5 (as well as Magi1) interact with delta-catenin in a phosphorylation-dependent manner and regulate dendritic branching (Baumert et al., 2020). The mouse knockout of Pdlim5 is embryonic lethal (Horiuchi et al., 2013) and Pdlim5's structure and presence is largely conserved across vertebrate animals (**Supplementary Figure 1A**) (e.g., ∼89% identity between human and rat). Dysregulation of Pdlim5 is proposed to factor into atypical dendritic tree morphology and synaptic connectivity in human neurodevelopmental diseases including schizophrenia, depression, and bipolar disorder (Kato et al., 2005; Horiuchi et al., 2006, 2013; Li et al., 2008; Liu et al., 2008; Zain et al., 2013) consistent with our *in vitro* studies identifying a regulatory role for Pdlim5 in dendrite morphology (Baumert et al., 2020).

Pdlim5 is composed of an N-terminal PDZ-domain (*PSD-95, D*lg, and *ZO*-1), central DUF-domain ("Domain of Unknown Function"), and a triad of C-terminal LIM-repeats (LIM domain) (**Figure 1B**; Nakagawa et al., 2000; Herrick et al., 2010). Pdlim5 is present in dendrites and other neuronal structures, with its subcellular distribution varying somewhat across developmental stages (Ren et al., 2015; Baumert et al., 2020). Pdlim5 is reported to associate with alpha-actinin and PKCepsilon and to be required in phorbol ester induced dendritic growth-cone collapse, restricting dendrite outgrowth in that context (Nakagawa et al., 2000; Ren et al., 2015). By having an inhibitory effect upon Rac to displace Arp2/3 from the leading edge, Pdlim5 also limits AMPK-stimulated cell migration in C2C12 cells via restriction of lamellipodia formation (Yan et al., 2015). In excitatory pyramidal hippocampal neurons, Pdlim5 inhibits formation of dendritic spines (via the inhibition of SPAR) (Herrick et al., 2010). In relation to gene activity, Pdlim5 affects neuron differentiation through cytoplasmic sequestration of the Id2 transcriptional regulator (Lasorella and Iavarone, 2006). In summary, Pdlim5 exhibits context-dependent positive and negative roles in dendrites, with Pdlim5 expression increasing dendritic arbor complexity as we have reported (Baumert et al., 2020).

Here, we reveal that Pdlim5 engages with a key partner protein, PalmD, in dendrite shaping. PalmD is of interest since it appears to be involved in membrane protrusion (Hultqvist et al., 2012; Kalebic et al., 2019) necessary to initiate dendrite branching. PalmD is also found to associate with adducin (Kalebic et al., 2019), a component of the spectrin-actin cytoskeleton that in turn acts in multiple cellular functions (Baines, 2010; Bennett and Lorenzo, 2016). Importantly, as demonstrated in this report, PalmD robustly passed our validation tests for association with Pdlim5, and it has attributes supporting a functional Pdlim5:PalmD relationship in dendrite branching.

Results

Pdlim5 is a positive regulator of dendritic branching

In our studies, we have employed mixed cultures of primary rat primary hippocampal neurons *in vitro*. This selection was made given their faithful reflection of key morphogenic properties

found *in vivo*, while at the same time offering facile manipulation for mechanistic and phenotypic tests. As outlined in Methods, we generally introduce control or experimental constructs into the cultured neurons at DIV1-3 (days *in vitro* 1-3) and fix at DIV5-7. Here, we assayed for endogenous protein expression as shown for Pdlim5 across DIV1-9. In unperturbed cells Pdlim5 is primarily evident in soma and neurites. It thus appears that in common with PalmD (see below **Figure 2**), Pdlim5 is available to make potentially-varied contributions across a series of neuronal developmental phases (e.g., from neurite through dendritic stages that are inclusive of initial through advanced branching events and synapse formation) (**Figure 1A**; see also **Figure 2**). Further, Pdlim5 and PalmD continue to be expressed in the adult CNS.[1] To form a baseline for subsequent phenotypic comparisons, we first built on our earlier findings demonstrating that the exogenous expression of Pdlim5 promotes dendrite branching of rat primary hippocampal neurons where we parallelly performed Map2 staining to identify dendrites (**Figures 1C, D**; Baumert et al., 2020). Sholl analysis of Map2 stained transfected neurons gave similar outcomes (results not shown), confirming dendritic identity. We complemented the exogenous expression phenotypes by conducting Pdlim5 knock-downs. Each of two independent siRNAs efficiently depleted Pdlim5 (**Supplementary Figures 1C, D**). Further, each siRNA severely reduced branching as seen in representative immunofluorescent images and as quantified by Sholl analysis (**Figures 1C, D**). Our findings here are entirely consistent with our prior work (Baumert et al., 2020) showing that Pdlim5 has a functional role in dendritic branching.

PalmD associates with Pdlim5, likely directly

To glean insight into candidate partners of Pdlim5, we undertook yeast two-hybrid (Y2H) screens of a mouse brain library (Hybrigenics, Inc.). Y2H screens of a chosen "bait" (e.g., Pdlim5) often provide initial clues pointing to direct interactions with "prey" proteins, and ours pointed to PalmD in the company of additional candidates (**Supplementary Figure 2**). Our interest focused on PalmD from the fact that little is known of its mechanisms of action, yet it has proposed roles in membrane protrusion, an early step in dendrite branching. Further, PalmD is thought to bind (via adducin) to the spectrin-actin cytoskeleton, a significant player in the shaping and functions of neurons (Li et al., 1998; Baines, 2010; Naydenov and Ivanov, 2011; Bennett and Lorenzo, 2016; Kalebic et al., 2019). While not pursued here, we note that also arising from our Y2H findings was alpha-actinin 4, an established crosslinker of actin microfilaments (Broderick and Winder, 2005; Thomas and Robinson, 2017) that was independently reported to associate with Pdlim5 (Nakagawa et al., 2000; Ren et al., 2015).

First, we looked at the relative degree of immunofluorescence colocalization of endogenous Pdlim5 and PalmD in rat primary hippocampal neurons (**Figures 2A, B**). Given that each neuron will go on to bear only one axon, we can assume that we primarily
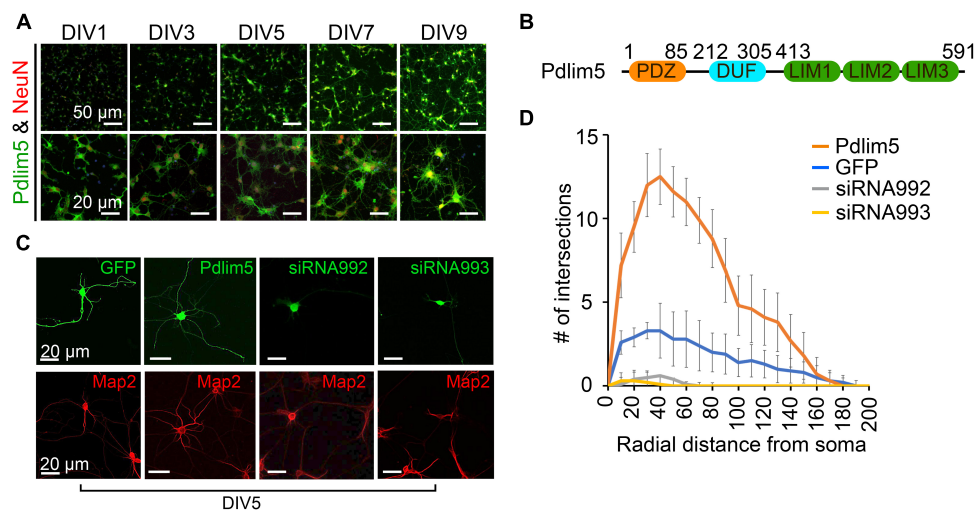
---

1   www.proteinatlas.org

FIGURE 1
Pdlim5 is a modulator of dendritic branching. **(A)** The images depict rat hippocampal neurons at different developmental stages (DIV1, DIV3, DIV5, DIV7, and DIV9). The neurons are stained for endogenous Pdlim5 (shown in green), the NeuN marker (shown in red) and DAPI (shown in blue), a marker for neuronal nuclei. The results presented [images in panels **(A,C)** and Sholl analysis in panel **(D)**] are representative of 3 biological replicates. **(B)** A diagram illustrating the major subdomains of Pdlim5. The N-terminus contains a PDZ domain (amino acids 1 to 85, shown in orange), followed by a domain of unknown function (DUF, amino acids 212 to 305, shown in cyan), and at the C-terminus, three LIM domains (amino acids 413 to 591, shown in green). **(C)** Immunofluorescent images demonstrating the effects on neuronal morphology of expressing GFP (negative control), Pdlim5-GFP, or siRNA constructs that were co-transfected with GFP targeting the knockdown of Pdlim5. Transfections occurred at DIV3 with fixation at DIV5. The images reveal a loss of neuronal complexity in cells subjected to Pdlim5 siRNA-mediated knockdown (siRNA992, siRNA993), while exogenous expression of Pdlim5 increases branching. Respective Map2 staining images are shown below (red). Representative images of three biological replicates. While not shown, Myc-Pdlim5 produced effects similar to Pdlim5-GFP when exogenously expressed. **(D)** Sholl analysis of neurons under the conditions: negative control (GFP), Pdlim5-GFP expression, and Pdlim5 siRNA-mediated knock down. Sholl analysis scores the number of dendrites that intersect a series of evenly spaced concentric rings (generated digitally during data processing) that radiate out from the cell-body/soma. The analysis indicates that compared to GFP-expressing cells (blue line), neurons exogenously expressing Pdlim5-GFP (orange line) exhibited a significant increase in the number of dendrites. Conversely, knockdown of Pdlim5 using siRNA (siRNA992, gray line; siRNA993, yellow line) shows loss of neuronal processes. Data points are the average values ($n \geq 15$ neurons) with error bars indicating standard error of the mean (SEM). The significance was assessed using a two-way ANOVA with Bonferroni *post hoc* analysis. Scale bars in the images represent 20 μm and 50 μm as indicated.

scored neurites destined to become dendritic processes. In other experiments as mentioned above this was further supported in that the processes being scored/examined exhibited Map2 staining. In DIV4 neurons, colocalization of Pdlim5 and PalmD was evaluated via immunocytochemistry, quantified by employing Mean Pearson's Coefficient. Values greater than zero are associated with positive correlations. In line with our expectation that Pdlim5 and PalmD form both paired and distinct complexes within cells, our findings are consistent with a significant but not complete overlap of their endogenous localizations.

We next quantitated the relative distributions of Pdlim5 and PalmD in the soma (cellular region immediately surrounding the nucleus), dendritic processes, and nuclei of DIV1&5 rat primary hippocampal neurons (**Figure 2E**). Given significant areas of co-presence, our findings were consistent with the possibility that these two proteins might form complexes within intracellular neuronal regions undergoing morphological differentiation. However, there remained the need to turn to additional assays for more definitive assessments of direct binding.

In this regard, we applied an approach that is familiar to us, proximity ligation assay (PLA) (Baumert et al., 2020). PLA points to very close protein:protein interactions ($\leq$30–40 nm) (Baumert et al., 2020). In common with our initial Y2H screen, PLA supported the likelihood of a direct Pdlim5:PalmD interaction relative to our negative and positive controls (**Figures 2C, D**).

For example, the Pdlim5:PalmD signals (puncta) observed were comparable in number and intensity to those resolved for our positive-control complex of Pdlim5:delta-catenin (Baumert et al., 2020). Overall, our Y2H and PLA findings were supportive of the proposed Pdlim5:PalmD association.

PalmD associates with Pdlim5 based upon endogenous co-IPs, as well as ectopic Golgi co-relocalization assays

We sought additional validations of the Pdlim5:PalmD association. For endogenous co-immunoprecipitations, we employed rat primary cortical neurons given their relative abundance in comparison to hippocampal neurons. Indeed, the immuno-precipitation of Pdlim5 produced a significant signal for associated PalmD (**Figures 3A, B**). The inverse co-IP was similarly supportive (**Supplementary Figure 3A**). Because endogenous Pdlim5 and PalmD migrate via SDS-PAGE at comparable positions, separate blots were used to resolve the co-IPs versus the self-IPs (**Supplementary Figure 3A**). We additionally assayed co-IPs of exogenous epitope-tagged constructs expressed in HEK293 cells, and we again readily resolved the Pdlim5:PalmD association (**Supplementary Figure 3B**). Our evidence suggests that the Pdlim5:PalmD association may be quite stable, as we found
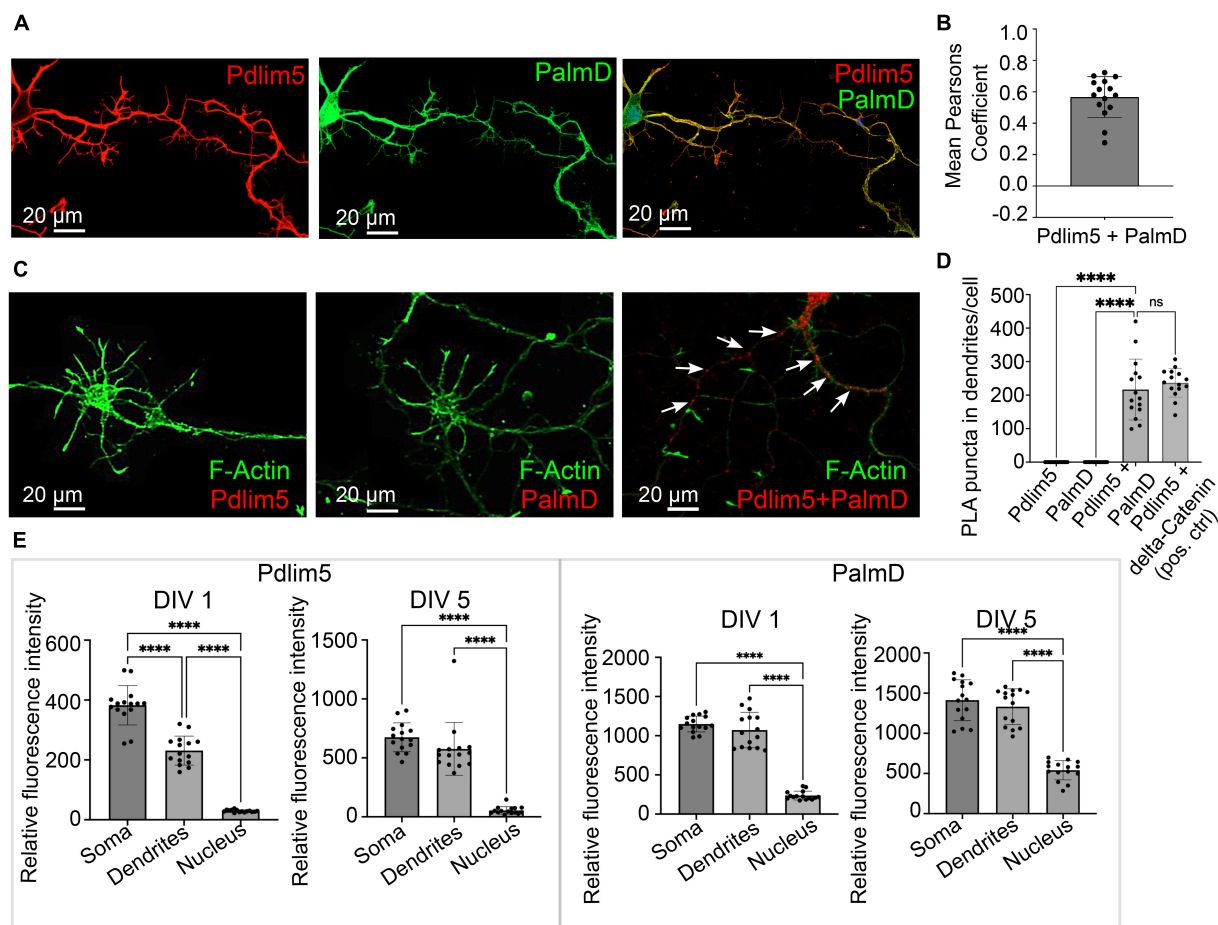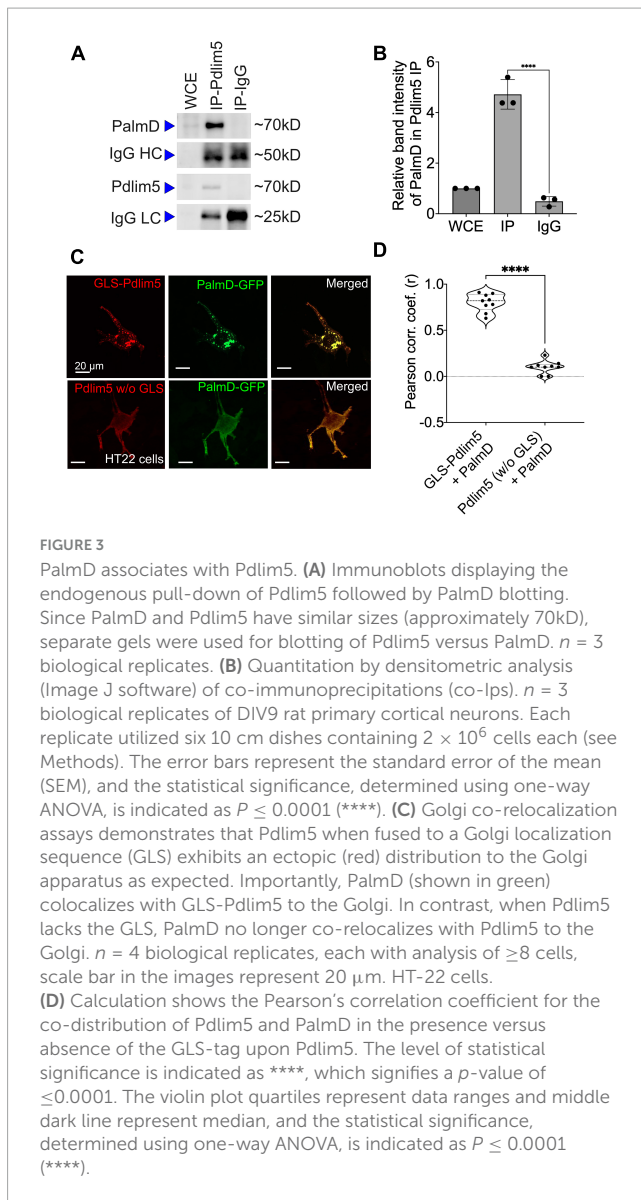
FIGURE 2

PalmD a novel partner of Pdlim5. **(A)** The image represents the colocalizations of Pdlim5 (shown in red), PalmD (shown in green) and DAPI (shown in blue) in rat hippocampal neurons at DIV4. Gross colocalization is indicated by the overlap color yellow in regions where both proteins are present within the same cellular compartment. Quantitation in Panel **(B)**. **(B)** The mean Pearson's coefficient was calculated to quantify the extent of colocalization between Pdlim5 and PalmD in neurites. The value 0.65 suggests significant (but not complete) linear correlation of Pdlim5 and PalmD colocalization within neurites. Three biological replicates were evaluated with similar outcomes (one shown), with data from ≥ 15 neurons each. Error bars indicate the standard error of the mean (SEM). Each dot in the graph represents one neuron. **(C)** Immunofluorescent image displays the results of a proximity ligation assay (PLA) of rat hippocampal neurons at DIV4, where the red-colored puncta indicate the positive reaction produced when antibodies to Pdlim5 and PalmD were employed. White arrows point to examples of positive (red) puncta while F-actin staining images shown side by side for Pdlim5 and PalmD (negative controls, green). Quantitation in Panel **(D)**. **(D)** The quantification of PLA puncta per cell observed in processes is plotted. Antibodies employed against endogenous Pdlim5 or PalmD alone served as negative controls, while the established endogenous complex of Pdlim5:delta-Catenin served as positive control. The data was collected from ≥ 15 neurons, with each dot representing one neuron. Three biological replicates were evaluated with similar outcomes (one shown). The error bars represent the standard error of the mean (SEM), and the statistical significance, determined using one-way ANOVA, is indicated as $P \leq 0.0001$ (****). ns, non significance. **(E)** The bar graphs compare the distribution of the Pdlim5 and PalmD proteins in different subcellular compartments, namely soma, neurites, and nucleus, in rat primary hippocampal neurons at two different developmental stages (DIV1 and DIV5). The relative fluorescence intensity for Pdlim5 and PalmD was quantified using ImageJ software. The data was obtained from 15 neurons, with each dot in the bar graph representing data from a single neuron. The error bars indicate the standard error of the mean (SEM). To determine the statistical significance, a one-way ANOVA analysis was performed using GraphPad Prism software. The levels of significance are indicated as **** for $P \leq 0.0001$, $n \geq 15$ neurons. Relative to the nucleus, this signifies high statistical significance of the observed subcellular localizations of both Pdlim5 and PalmD to neurites and soma in rat hippocampal neurons.

the complex routinely survived even overnight incubations in cell lysis/extraction buffer.

To apply a further test, we took an orthogonal approach that we earlier developed (Baumert et al., 2020). In it, one's construct of interest is ectopically directed to the outer Golgi membrane *via* fusion to a Golgi localization sequence (GLS). A putative partner is then co-expressed, and we score for its ectopic co-targeting, versus not, to the Golgi (we assess if the partner "comes along for the ride"). An attractive aspect of this method is that potential associations are happening

in the cell cytoplasm without biochemical treatment for lysis. Thus, the interactions are maintained in a more natural intra-cellular environment. We resolved strong Pdlim5:PalmD colocalization to Golgi when Pdlim5 was ectopically localized there *via* fusion to a GLS, but not when Pdlim5 lacked such a GLS (negative control) (Figure 3D). These experiments were conducted in HT-22 cells (immortalized mouse hippocampal neuronal cell line), as we found them amenable to Golgi visualization/scoring. In summary, both our co-IP and GLS tests confirm Pdlim5:PalmD association (Figure 3), as originally

FIGURE 3

PalmD associates with Pdlim5. **(A)** Immunoblots displaying the endogenous pull-down of Pdlim5 followed by PalmD blotting. Since PalmD and Pdlim5 have similar sizes (approximately 70kD), separate gels were used for blotting of Pdlim5 versus PalmD. $n = 3$ biological replicates. **(B)** Quantitation by densitometric analysis (Image J software) of co-immunoprecipitations (co-Ips). $n = 3$ biological replicates of DIV9 rat primary cortical neurons. Each replicate utilized six 10 cm dishes containing 2×10^6 cells each (see Methods). The error bars represent the standard error of the mean (SEM), and the statistical significance, determined using one-way ANOVA, is indicated as $P \leq 0.0001$ (****). **(C)** Golgi co-relocalization assays demonstrates that Pdlim5 when fused to a Golgi localization sequence (GLS) exhibits an ectopic (red) distribution to the Golgi apparatus as expected. Importantly, PalmD (shown in green) colocalizes with GLS-Pdlim5 to the Golgi. In contrast, when Pdlim5 lacks the GLS, PalmD no longer co-relocalizes with Pdlim5 to the Golgi. $n = 4$ biological replicates, each with analysis of ≥ 8 cells, scale bar in the images represent 20 μm. HT-22 cells. **(D)** Calculation shows the Pearson's correlation coefficient for the co-distribution of Pdlim5 and PalmD in the presence versus absence of the GLS-tag upon Pdlim5. The level of statistical significance is indicated as ****, which signifies a p-value of ≤ 0.0001. The violin plot quartiles represent data ranges and middle dark line represent median, and the statistical significance, determined using one-way ANOVA, is indicated as $P \leq 0.0001$ (****).

supported via yeast 2-hybrid (Y2H) and proximity ligation assays (PLA) (**Figure 2**).

We went on to apply the GLS methodology to map the region of Pdlim5 that binds to PalmD. Varied constructs of Pdlim5 were tested that retained or lacked each of Pdlim5's three principal domains: PDZ, DUF, and LIM (**Supplementary Figure 3**). Our findings clearly indicated a primary role of Pdlim5's C-terminal LIM domain in PalmD association, as opposed to the N-terminal PDZ or central DUF domains (**Supplementary Figure 3D**). This result was further supported using traditional co-IP strategies, where the LIM domain was found to co-IP with PalmD (**Supplementary Figure 3C**).

Functional assays support Pdlim5's relationship with PalmD

Analogous to what was earlier indicated in **Figures 1A** with regards to the developmental presence of Pdlim5 in rat

hippocampal neurons (DIV1-9), PalmD is readily observed in dendrites and soma (**Figure 4A**; see also **Figure 2**). Using both exogenous expression and knock-down approaches we addressed the impact of manipulating the levels of PalmD in rat primary hippocampal neurons. Upon its exogenous expression, we found that PalmD potently enhanced dendritic branching as quantified via Sholl analysis, while conversely, PalmD knockdown using two independent siRNAs had the opposing impact, dramatically reducing such branching (**Figures 4B, C**). Similar exogenous expression and knockdown effects were observed when applying other measurements such as counting the number of dendritic tips or branch points per primary hippocampal neuron, or when using Imaris-generated 3-D renderings or binary images for visualizations (**Supplementary Figure 4**). This suggested to us that the Pdlim5 and PalmD components within the Pdlim5:PalmD complex are positive modulators of branching.

We next asked if the effects observed upon expressing Pdlim5 was dependent on the presence of PalmD, and vice versa. When Pdlim5 was exogenously expressed under conditions of PalmD knockdown, we failed to observe any enhancement of branching (**Figures 4D, E**). Indeed, as seen with the knockdown of PalmD-alone, we observed suppression of branching relative to the GFP-alone control. We likewise observed that the promotion of dendrite branching upon PalmD expression became suppressed upon the parallel knockdown of Pdlim5 (**Supplementary Figures 4E, F**). These findings are consistent with the existence of not only a biochemical Pdlim5:PalmD complex but also a functional dependence between Pdlim5 and PalmD in the process of dendritic branching.

Discussion

The complexity of neuronal interconnections allowing for vertebrate central nervous system functions is impressive by any standard, and there remains much to be learned about how dendrites are shaped to enable such interconnections. Generally, neuronal networking requires the control of dendrite morphology because neuron:neuron interactions depend upon the precise postsynaptic contacts of each dendrite's associated synaptic spines. The postsynaptic specializations of dendrites receive signals from the presynaptic terminals of axons that extend from nearby or distal neurons. In this report, we focused upon the gross shaping of dendrites as opposed to the formation of precise synaptic contacts, but these vastly different morphologic scales remain interrelated given that proper synapse patterning can only come about when dendrites adopt morphologies consistent with spine/synapse generation. There are numerous extrinsic and intrinsic cellular factors that modulate neuronal branching. With regards to extrinsic cues, glutamate (Portera-Cailliau et al., 2003; Rusakov and Stewart, 2021) and brain derived neurotrophic factor (BDNF) (Popova et al., 2017) are just two examples, along with varied transmembrane ligand:receptor pairings inclusive of cell:cell adhesion molecules (Dong et al., 2015; Valnegri et al., 2015). Prominent intrinsic cellular factors include examples like small-GTPases, cytoskeletal components or regulators (e.g., affecting organelle distribution and the extent or polarity of vesicular traffic), and varied intracellular or junctional signaling entities (Puram and Bonni, 2013). Nuclear
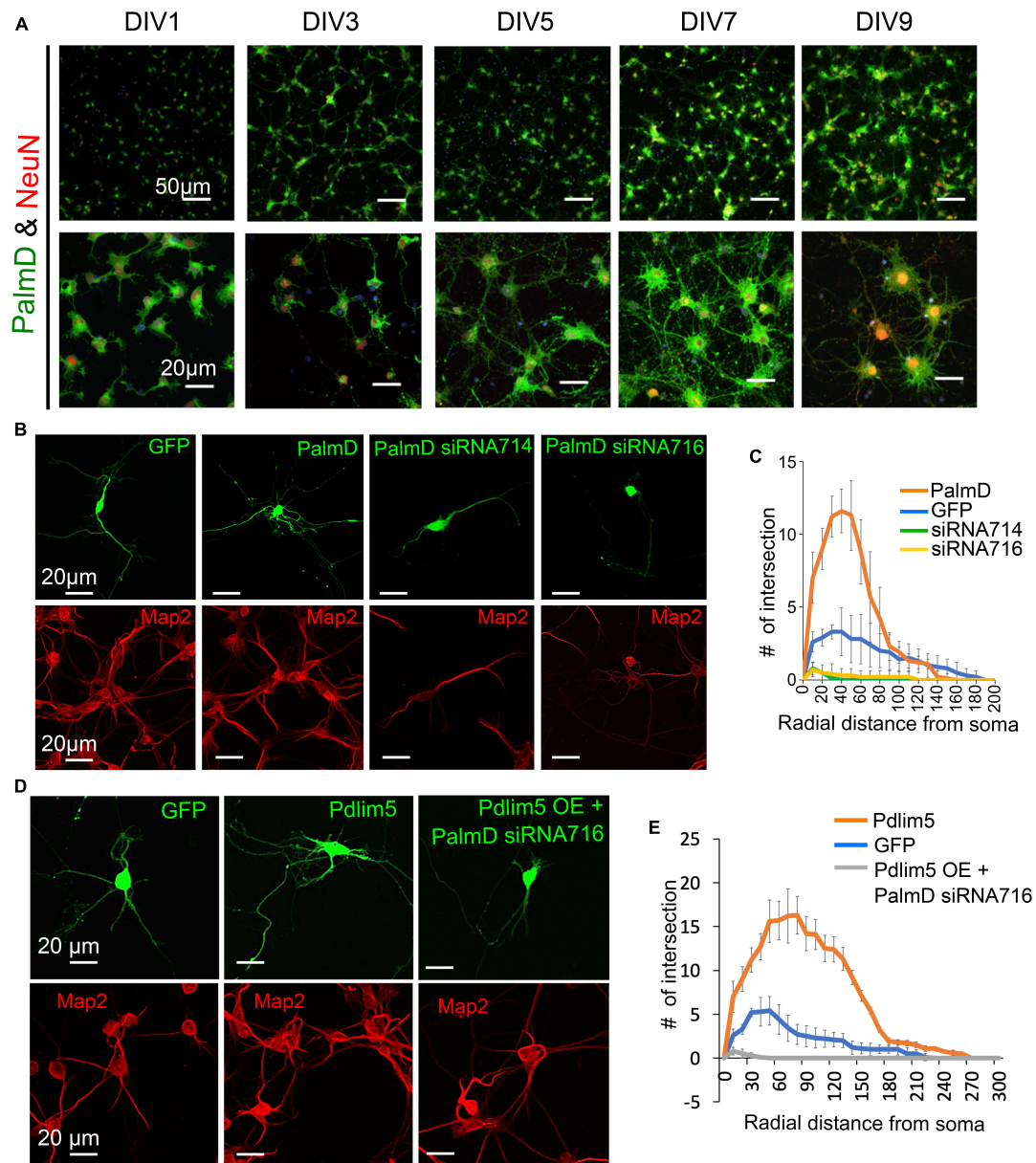
FIGURE 4

PalmD characterization and its functional dependency with Pdlim5. **(A)** Rat primary hippocampal neurons at the indicated developmental stages (DIV1, DIV3, DIV5, DIV7, and DIV9), are immuno-stained for endogenous PalmD (shown in green), the NeuN marker (shown in red), which identifies neuronal nuclei, and DAPI (shown in blue), n = 3 biological replicates. The scale bars in the images indicate 20 μm and 50 μm. **(B)** These immunofluorescent images illustrate the impact of PalmD-GFP exogenous expression versus siRNA-mediated knockdown of PalmD (siRNA714, siRNA716) on neuronal morphology. Respective Map2 staining images are shown below (red) PalmD siRNA-mediated knockdown decreases process complexity, while exogenous expression increases branching morphology. Three biological replicates in each condition analyzing ≥ 15 neurons. Quantitation present in Panel **(C)**. While not shown, flag-PalmD produced effects similar to PalmD-GFP when exogenously expressed. **(C)** Sholl analysis was conducted to examine the dendrite morphology of neurons under different conditions: namely negative control (GFP, blue line), PalmD-GFP exogenous expression (orange line), and PalmD siRNA-mediated knock down (siRNA714, green line; siRNA716, yellow line). The analysis demonstrates that neurons overexpressing PalmD-GFP exhibit a significant increase in dendritic complexity, while knockdown of PalmD results in severe reductions. The significance was assessed using a two-way ANOVA with Bonferroni *post hoc* analysis that varies from $P \leq 0.0001$ and $P < 0.05$, based on radial distance from the cell soma (compared to cells expressing GFP alone). The error bars represent the standard error of the mean (SEM). $n \geq 15$ neurons in each of three biological replicates. **(D)** Functional interdependence of Pdlim5 and PalmD. The panel indicates the GFP control (green) condition relative to Pdlim5-GFP exogenous expression (green), and versus Pdlim5-GFP exogenous expression (green) in the presence of PalmD siRNA-mediated knockdown (KD). Respective Map2 staining images are shown below (red). The results suggest an interdependence between Pdlim5 and PalmD in regulating neuronal morphology. Analyzed ≥ 15 neurons in each of three biological replicates. See panel **(E)** for quantitation. **(E)** Sholl analysis was performed to analyze dendrite morphology under different conditions: GFP control, Pdlim5-GFP exogenous expression, and Pdlim5-GFP exogenous expression with concomitant knock down of PalmD (siRNA716). The analysis reveals that neurons overexpressing Pdlim5-GFP (orange line) exhibit increased numbers of dendrites compared to control GFP-expressing cells (blue line) ($P \leq 0.0001$ and $P < 0.05$ for the respective regions 20−90 μm and 110−170 μm from the soma). However, when PalmD siRNA716 is introduced alongside Pdlim5-GFP exogenous expression (gray line), there is a significant loss of branching function. The error bars represent the standard error of the mean (SEM). $n \geq 15$ neurons each from three biological replicates. The significance was assessed using a two-way ANOVA with Bonferroni *post hoc* analysis.

contributions (e.g., transcriptional) are also relevant in establishing gross or refined morphologies but their varied effects are generally viewed as being more indirect.

Using rat primary hippocampal neurons, we here reveal that increasing PalmD levels heightens dendritic branching, while decreasing PalmD has the opposite effect. PalmD has been suggested to engage in shaping membranes, potentially by enhancing their curvature while facilitating intracellular interactions with actin-based processes (Hultqvist et al., 2012; Kalebic et al., 2019). Such a possibility is consistent with properties ascribed to related family members of PalmD such as paralemmin (Kutzleb et al., 1998; Gauthier-Campbell et al., 2004; Arstikaitis et al., 2008; Fukata and Fukata, 2010), for which C-terminal palmitoylation and thereby enhanced membrane localization was indicated to promote neuronal process complexity. Recently, PalmD was reported to promote process formation in the basal progenitor cells of the mammalian neocortex (Kalebic et al., 2019). In that work, PalmD bearing a C-terminal Caax motif was proposed to achieve membrane localization via Caax palmitoylation in line with its activity in process formation. Our findings were instead derived from differentiated rat hippocampal and cortical neurons. They indicate that even a PalmD isoform lacking the C-terminal Caax motif [isoform having four terminal KKVI residues instead (Hu et al., 2001; Kalebic et al., 2019)] remained robustly capable of advancing dendritic branching. In the neuronal context, one possibility is that PalmD lacking its C-terminal Caax motif might still become palmitoylated or otherwise lipidated elsewhere within its structure. This could enable PalmD's presence and interactions at presumptive or forming dendritic membranes to advance branching processes. Alternatively, a fraction of PalmD might become membrane localized through its direct association with Pdlim5 or other potential membrane associated binding partners. Membrane localization was artificially reflected here using an experimental approach we earlier devised (GLS assay) (Baumert et al., 2020). In it, we targeted Pdlim5 to the Golgi and demonstrated co-targeting of PalmD, that is, Palm D came along for the ride. In normal neuronal contexts, the PDZ-domain of Pdlim5 is capable of binding to multiple proteins bearing PDZ-motifs, presumably including that proportion of delta-catenin at dendritic membranes (Baumert et al., 2020). Other possibilities to consider as tethers to the membrane-cytoskeleton include adducin (Kalebic et al., 2019), as well as potentially indirect interactions of PalmD with alpha-actinin or cortactin (see below). In all cases, while beyond the scope of our report here, future work in the field is required to address PalmD's downstream mechanisms of action, inclusive of its indirect associations with the inner dendritic membrane or with relevant cytoskeletal elements.

Using multiple orthogonal tests, we provide evidence of PalmD's association with Pdlim5, a scaffold that we earlier characterized in association with delta-catenin (Baumert et al., 2020). Each of these three proteins enhance dendrite branching when exogenously expressed alone, and conversely, the knockdown of each individual gene product alone leads to neurons having a greatly reduced presence of dendritic processes. delta-Catenin is thought to promote dendrite branching in part through inhibition of the small-GTPase RhoA (Martinez et al., 2003; Abu-Elneel et al., 2008; Gu et al., 2009; Donta et al., 2022), which we have

likewise indicated is the case for Pdlim5 (Baumert et al., 2020). Given that PalmD associates with Pdlim5, there is the possibility that PalmD's effects may likewise involve RhoA or another small-GTPase. Further potential links of PalmD to cytoskeletal modulation revolve around the presence of additional associated proteins in complex with Pdlim5 or with delta-catenin. For example, associations based upon the respective interactions of Plim5 and delta-catenin with the potent cytoskeletal regulators alpha-actinin (Nakagawa et al., 2000; Ren et al., 2015) and cortactin (Martinez et al., 2003; Abu-Elneel et al., 2008), each known to contribute to the production or maintenance of cellular processes. Thus, while conjectural at this stage, a number of possible downstream mechanisms of action could be proposed based upon established associations of PalmD's direct or indirect protein partners.

Our prior work (Baumert et al., 2020) and that of others (Abu-Elneel et al., 2008) outlines what could be a key upstream pathway that impinges on the Pdlim5:PalmD complex revealed here, with consequent effects upon gross dendritic morphology. Specifically, Pdlim5's (and thereby PalmD's) association with delta-catenin is determined by a "phospho-switch" at the very C-terminus of delta-catenin. As reflected in this report's Graphical Abstract, the phosphorylation of delta-catenin is responsive to upstream glutamate signaling via the neuronal mGluR5 receptor and consequent activation of Cdk5 kinase (Baumert et al., 2020). Even as future work will be needed to precisely identify the cytoskeletal players downstream of the delta-catenin:Pdlim5:PalmD complex, we speculate as noted the direct involvement of cortactin, alpha-actinin 4, and RhoA inhibition, as well as the spectrin network and membrane-curvature agents. In summary, we unveil here a novel Pdlim5:PalmD complex that associates with delta-catenin, which through functional interdependencies, promotes dendritic branching-morphology required in development and is aberrant (see Introduction) in multiple pathological contexts.

Materials and methods

Neuronal cultures and transfection

Primary hippocampal and cortical neurons were obtained from rat embryos at the 18th day of gestation (E18), following methodology previously described in Fischer et al. (2018) and Gireud-Goss et al. (2020). Subsequent to isolation, the hippocampal neurons were plated in 24-well tissue-culture plates at a density of 2×10^5 cells per well. To facilitate adhesion, glass coverslips within the wells were pre-coated with 100 µg/ml poly-D-lysine (Sigma-Aldrich). Cortical neurons were plated at 20×10^6 cells per 10 cm Petri dish pre-coated with 100 µg/ml poly-D-lysine. The cultured hippocampal neurons were maintained in Neurobasal Medium (Life Technologies), supplemented with B-27, GlutaMAX, and penicillin-streptomycin (each from Life Technologies). At 3 days *in vitro* (DIV3), the neurons underwent Lipofectamine 2000 based transfection using the manufacturer's protocol (Life Technologies) but employing 1 µg plasmid DNA while at 7 days *in vitro* (DIV7) cells were fixed for immunostaining.

HEK293 cell culture and transfection

HEK293 cells from ATCC (ATCC# CRL-1573) were cultured in DMEM cell culture media (Sigma-Aldrich) supplemented with 10% FBS (Sigma-Aldrich) and 1x penicillin-streptomycin (Life Technologies). Media change was performed every other day until the cells reached 80% confluency, after which they were transferred to new culture dishes. Transfection of the HEK293 cells with exogenous DNA (1 μg) was accomplished using Lipofectamine 2000 as per the manufacturer's instructions. Transfection took place when the cells reached 50–60% confluency in six-well culture plates. Co-IPs were conducted as below mentioned.

cDNA constructs

All cDNA constructs were cloned into the backbone of the pCS2 mammalian expression vector. Engineering was undertaken by Epoch Life Science and/or the McCrea laboratory. All constructs were confirmed with DNA sequencing. The full length PalmD-pCMV6-AC-GFP was purchased from Origene (RG203079), and PalmD-GFP was moved into the pCS2 vector. Pdlim5 was engineered previously in our laboratory (Baumert et al., 2020). DNA maxi-preps were outsourced to Epoch Life Sciences. See Table 1 for a complete list of constructs and their corresponding epitope tags/fusions.

siRNAs

To synthesize and validate siRNAs that target Pdlim5 or PalmD, we first identified corresponding 19-nucleotide target sequences using the siRNA Wizard v3.1 tool from InvivoGen. Two siRNAs were selected for each target to enable the generation of siRNAs. The siRNA sequences for Pdlim5 were 5′-GCACUGUAUUGUGAGCUAUtt-3′ and 5′-CAACUGUGCUCACUGCAAAtt-3′, while for PalmD they were 5′-GCAUCAGGCAGAACGAAUAtt-3′ and 5′-CGAGGAUAUCUAUGCUAAUtt-3′.

siRNAs for Pdlim5 and PalmD were purchased from Life Technologies. Individual siRNAs were transfected into hippocampal neurons using the manufacturer's Lipofectamine 2000 protocol. Neurons were allowed to grow for 24–48 h before conducting immunofluorescence assays. Knockdown efficiency of each siRNA was assessed using immunocytochemistry with anti-Pdlim5 or anti-PalmD primary antibodies, and IMARIS software was used to quantify the intensity of immunostained images. Sholl analysis was used to assess the impact upon neuronal morphology (see below).

Antibodies

Antibodies that recognize specific epitope tags as well as endogenous proteins were obtained commercially. Rabbit polyclonal anti-Myc epitope-tag (MT) antibodies (Cell Signaling Technology/CST #2272S), mouse monoclonal anti-Myc epitope-tag (MT) antibodies (CST #9B11), anti-GFP antibodies (CST #2956

TABLE 1 Star methods: key resources table.

Reagent or resources	Source	Identifier
Constructs		
PalmD-GFP	Origene	RG203079
6x Myc Pdlim5 full length (6MT Pdlim5 FL)	McCrea's Lab	NA
Pdlim5_isolated 6x Myc PDZ (6MT PDZonly)	Epoch Life Science	NA
Pdlim5_isolated 6x Myc DUF (6MT DUFonly)	Epoch Life Science	NA
Pdlim5_isolated 6x Myc LIM (6MT LIMonly)	Epoch Life Science	NA
Pdlim5_isolated 3x flag PDZ (3xflag PDZonly)	Epoch Life Science	NA
Pdlim5_isolated 3x flag DUF (3xflag DUFonly)	Epoch Life Science	NA
Pdlim5_isolated 3x flag LIM (3xflag LIMonly)	Epoch Life Science	NA
Pdlim5 siRNA993	Life Technology	S133993
Pdlim5 siRNA992	Life Technology	S133992
PalmD siRNA714	Life Technology	S160714
PalmD siRNA716	Life Technology	S160716
Cell culture		
DMEM	Corning	10-017-CV
Opti-MEM	Gibco	31985-070
DPBS 1X	Corning	21-031-CV
Trypsin-EDTA	Sigma	T4049
Poly-D-Lysine/Laminin Cell ware 12mm round coverslips	Corning	354087
Penicillin-Streptomycin solution 100X	GenDEPOT	CA005-010
Chemicals		
Bovine Serum Albumin	Sigma	A3059
HEPES	Gibco	15630-080
TEMED	Bio-Rad	161-0801
Acrylamide 30% solution	Sigma	A3699
Complete Tablet, Mini, EDTA-free protease inhibitor cocktail	Roche	04693159001
PhosSTOP phosphatase inhibitor cocktail	Roche	04906845001
Vectashield	Vector Laboratories	H-1000
DPBS 10X	Sigma	D1408
Formaldehyde 4% in PBS	Alfa Aesar	J60401-AP
Restore PLUS western blot stripping buffer	Thermo Scientific	46430
Resolving Gel Buffer	Bio-Rad	1610798
NONIDET P-40	ICN Biomedicals	9016-45-9
2x Laemmli Sample	Bio-Rad	161-0737
2-Mercaptoethanol	Bio-Rad	161-0710
Premium Microscope Slides superfrost	Fisher Scientific	22-178-277
Ammonium persulfate	Sigma-Aldrich	248614
Sodium Chloride	Fisher Scientific	S271-3

(Continued)

TABLE 1 (Continued)

Reagent or resources	Source	Identifier
Tris Base	Fisher Bioreagents	BP152-500
Glycine	MP Biomedicals	194681
Whatman Protran BA 83	GE Healthcare Life Sciences	10401396
Antibodies		
Anti-Myc mouse monoclonal	Cell Signaling Technology (CST)	9B11
Anti-Myc rabbit polyclonal	CST	2272S
Anti-FLAG rabbit polyclonal	Sigma	F7425
Anti-GFP mouse monoclonal	CST	4B10
Anti-GFP rabbit polyclonal	CST	2956
Anti-Pdlim5 mouse monoclonal	Thermo Fisher Scientific	MA5-25915
Anti-Pdlim5 mouse monoclonal	Sigma Aldrich	WH0010611M1
Anti-Pdlim5 rabbit polyclonal	Thermo Fisher Scientific	38–8800
Anti-PalmD rabbit polyclonal	ProteinTech	16531-1-AP
Anti-delta-catenin mouse monoclonal	BD transduction laboratories	611537
Anti-NeuN rabbit polyclonal	Invitrogen	PA5-78499
Anti-NeuN mouse monoclonal	Invitrogen	MA5-33103
Alexa fluor 488 goat polyclonal anti-mouse IgG	Invitrogen	A32723
Alexa fluor 488 goat polyclonal anti-rabbit IgG	Invitrogen	A11008
Alexa fluor 555 goat polyclonal anti-mouse IgG	Invitrogen	A21422
Alexa fluor 555 goat polyclonal anti-rabbit IgG	Invitrogen	A32732
Anti-Map2 chicken polyclonal	Thermo Fisher Scientific	PA1-10005
Alexa fluor 555 goat anti-chicken IgY	Invitrogen	A32932
Software		
IMARIS 9.9	Oxford Instruments	NA
Image J	FIJI	NA
Prism 9	GraphPad Software	NA

Further information and requests for resources should be directed to the Lead Contact, PM.

from rabbit and CST #4B10 from mouse), and a mouse monoclonal anti-FLAG epitope-tag antibody (Sigma #F7425). For the detection of endogenous Pdlim5, two mouse monoclonal antibodies were utilized: one for the purpose of IP/immuno-blotting (Thermo Fisher Scientific catalog # MA5-25915) (**Figure 3A**; **Supplementary Figure 3A**), with a second mouse monoclonal (Sigma-Aldrich catalog # WH0010611M1) used to detect endogenous Pdlim5 via immunofluorescence (**Figure 1A**). A rabbit polyclonal antibody directed against Pdlim5 (#38–8800) was used for both blot and immunofluorescence (IF) assays. Primary rabbit IgG from Life Technologies (#10500C) were used for negative-control "IPs," as was mouse IgG from Invitrogen (#10400C) (**Figure 3A**,

Supplementary Figures 3A–C). To detect endogenous PalmD in immunofluorescence assays, we employed a rabbit polyclonal antibody (ProteinTech, catalog # 16531-1-AP) (**Figure 3A**; **Supplementary Figure 3A**). delta-Catenin was visualized using a mouse monoclonal antibody (BD Transduction Laboratories catalog # 611537, not shown). All HRP-conjugated goat polyclonal secondary antibodies were obtained from Thermo Fisher Scientific (anti-mouse #31430 and anti-rabbit #31460). All Alexa fluor immunofluorescent secondary antibodies were purchased from Invitrogen (488 anti-mouse #A32723, 488 anti-rabbit #A22008, 555 anti-mouse #A21422, 555 anti-rabbit #A32732 and 555 anti-chicken A32932).

Golgi localization sequence assay

Immortalized mouse hippocampal neuronal cells (HT-22) were cultured in DMEM cell culture media (Sigma-Aldrich) supplemented with 10% FBS (Sigma-Aldrich) and 1x penicillin-streptomycin (Life Technologies). Transfections of cells were done at 50–60% confluency using Lipofectamine 2000. Golgi co-relocalization was examined by fixation with 4% PFA 24 h after transfection, followed by immunostaining and subsequent image collection using confocal microscopy. To ectopically relocalize Pdlim5 to the Golgi, Pdlim5 was tagged at its' N-terminus with the Golgi localization sequence (GLS) of mammalian target of rapamycin (mTOR) (Baumert et al., 2020). Following co-transfection with one of Pdlim5's putative partners (e.g., PalmD), the cells were subjected to immunofluorescence staining as previously described (Baumert et al., 2020; Donta et al., 2023). Qualitative analysis involved visual examination of co-relocalized partner proteins to the Golgi, occurring only when GLS-Pdlim5 is present. Quantitative analysis involved measuring the average fluorescence intensity of the Golgi body compared to that of the cytosol in each optical channel using ImageJ. This comparison generated a Golgi:cytosolic intensity ratio for each condition.

GLS from mammalian target of rapamycin: 5′-ACTAGT GAAATGCTGGTCAACATGGGAAACTTGCCTCTGGATGAGT TCTACCCAGCTGTGTCCATGGTGGCCCTGATGCGGATCTT CCGAGACCAGTCACTCTCTCATCATCACACCATGGTTGTC CAGGCCATCACCTTCATCTTCAAGTCCCTGGGACTCAAAT GTGTGCAGTTCCTGCCCCAGGTCATGCCCACGTTCCTTAA CGTCATTCGAGTCTGTGATGGGGCCATCCGGGAATTTTTG TTCCAGCAGCTGGGAATGTTGGTGTCCTTTGTGAAGAGC CACATCAGACCTTATATGGATGAAATAGTCACCCTCATGA GA-3′.

PLA

To perform Proximity Ligation Assays (PLA), neurons were fixed at 4 days *in vitro* (DIV4) with 4% PFA and the Duolink PLA kit was employed as previously described (Baumert et al., 2020) following the manufacturer's (Sigma-Aldrich) protocol (Alam, 2018).

In brief, cells were permeabilized with 0.5% Triton-X 100 and blocked with 1% BSA blocking solution. Neurons were then incubated with primary antibodies specific to each of the

two endogenous target proteins, such as Pdlim5 and PalmD. Subsequently, the cells were washed with PBS and incubated with Duolink PLA probes. These probes recognize the primary antibodies and enable the generation of a DNA structure recognized by manufacturer-provided fluorescent probes. To generate the DNA structure, the cells were incubated with a ligase and amplification enzymes. Finally, the permeabilized and blocked cells were incubated with the fluorescent probes and imaged using a Nikon T2i Inverted Confocal Microscope equipped with an Apo-Plan 60 × 1.4 NA oil objective. The imaging was conducted at a pixel size of 100 nm, and image stacks were converted into maximum projection images for analysis. The quantification of puncta was performed using the Puncta Analyzer plugin within the ImageJ software.

Co-immunoprecipitations and immunoblots

For immunoblot assay of endogenous proteins from rat primary cortical neurons, 2×10^6 cells from six 10 cm dishes were collected and lysed at DIV9. For immunoblotting assays of exogenous co-immunoprecipitated proteins, HEK293 cells were lysed 24–48 h following their co-transfection, using established protocols (Baumert et al., 2020). In brief, following lysis and pelleting of debris, protein concentrations of lysates were equalized (500–1000 μg per condition/IP) and incubated with primary antibodies for 2–12 h at 4°C with gentle rotation. Protein-A and Protein-G Dynabeads (Invitrogen, #10002D and #10004D) were added to each tube and incubated for an additional 20–30 min with gentle rotation at 4°C. After washing, the associated proteins were eluted from the beads upon addition of 2 × sample buffer with βME and heated at 95°C for 5 min. Co-IP samples, or in the case of whole-cell extracts equalized cell lysates, were then loaded onto 10% polyacrylamide gels using a BioRad mini-PROTEAN Tetra Cells, 2-gel system setup (#1658005) and run for 120 min. Proteins were then transferred to nitrocellulose membranes (GE Whatman) using a Pierce Power Blotter (Thermo Fisher Scientific). Membranes were blocked in TBS supplemented with 0.1% Tween-20 plus 1% dry milk, with incubation for 4–12 h at 4°C. Blocked membranes were incubated in primary antibodies overnight at 4°C before being incubated with HRP-conjugated secondary antibodies (Invitrogen) for 1–2 h at room temperature. Lastly, membranes were incubated with Pierce ECL immuno-blotting substrate (Thermo Fisher Scientific # 32106) and imaged using a ChemiDoc MP imaging system (Bio-Rad).

Immunofluorescence staining and confocal microscopy

Immunostaining of rat primary hippocampal neurons or HT-22 cells employed established protocols (Baumert et al., 2020). Briefly, cells cultured on poly-D-lysine-coated coverslips were fixed with 4% paraformaldehyde for 10 min at room temperature and then permeabilized with 0.5% Triton X-100 solution for 15 min. Following fixation and permeabilization, cells were blocked with

PBS containing 1% bovine serum albumin overnight at 4°C. Cells were then incubated with the indicated primary antibodies overnight at 4°C and subsequently rinsed three times with fresh PBS for 10 min each, followed by an overnight rinse with PBS at 4°C. Cells were then incubated with Alexa Fluor fluorescent dye-conjugated secondary antibodies (Invitrogen) for 1 h at room temperature before the coverslips were washed and finally mounted onto glass slides with Vectashield (Vector Laboratories) mounting solution. Cells were visualized using a Nikon T2i Inverted Confocal Microscope with an Apo-Plan 60 × 1.4 NA oil objective at room temperature. Images were captured with a Nikon A1-DUG GaAsP hybrid four-channel multi-detector and Nikon NIS-Elements software. All z-series images were acquired at a pixel size of 100 nm and a step size of 0.2 μm.

Neuronal morphological analysis by IMARIS9.9

Rat primary hippocampal neurons underwent assessment of their morphological characteristics with a focus upon neurites/dendrites. z-Series images of immunofluorescently stained neurons were captured using a Nikon T2i Inverted Confocal Microscope, as previously mentioned. Prior to analysis, IMARIS 9.9 was utilized to generate a 2-dimensional maximum-projection image with background subtraction from the confocal z-series of each neuron. In cases where dendrite number was evaluated, counting focused upon the number of dendrite tips per neuron, excluding any protrusions shorter than 5 μm. Dendritic length was measured by tracing from the cell body to the tip of the dendrite using IMARIS 9.9 filament tracer. Thresholds and settings for IMARIS 9.9 filament tracer were kept the same for all samples. For Sholl analysis, the maximum-projection images were converted to binary and analyzed in IMARIS 9.9 filament tracer using concentric rings with a 5 μm step size to evaluate dendrite morphology in relation to the distance from the cell body (Donta et al., 2023).

Statistical analysis

Data were analyzed using GraphPad Prism. Statistical significance for Sholl data were determined using a two-way ANOVA with Bonferroni *post hoc* analysis (Figures 1D, 4C, E; Supplementary Figure 4E). For all other comparisons, a one-way ANOVA with Tukey's test was used (Figures 2B, D, E, 3B, D; Supplementary Figures 1B, D, 4B–D). Data distribution was assumed to be normal, but this was not formally tested. Significance was assigned at $P < 0.05$. Please refer to each Legend for specific information related to experimental statistical considerations.

Data availability statement

The raw data supporting the conclusions of this article will be made available by the authors, without undue reservation.

Ethics statement

The animal study was approved by the Center for Laboratory Animal Medicine and Care, at the University of Texas Health Science Center, Houston. The study was conducted in accordance with the local legislation and institutional requirements.

Author contributions

Funding

Acknowledgments

Conflict of interest

The authors declare that the research was conducted in the absence of any commercial or financial relationships that could be construed as a potential conflict of interest.

Publisher's note

All claims expressed in this article are solely those of the authors and do not necessarily represent those of their affiliated organizations, or those of the publisher, the editors and the reviewers. Any product that may be evaluated in this article, or claim that may be made by its manufacturer, is not guaranteed or endorsed by the publisher.

Supplementary material

The Supplementary Material for this article can be found online at: https://www.frontiersin.org/articles/10.3389/fncel.2024.1315941/full#supplementary-material

References

Abu-Elneel, K., Ochiishi, T., Medina, M., Remedi, M., Gastaldi, L., Caceres, A., et al. (2008). A delta-catenin signaling pathway leading to dendritic protrusions. *J. Biol. Chem.* 283, 32781–32791. doi: 10.1074/jbc.M804688200

Alam, M. S. (2018). Proximity ligation assay (PLA). *Curr. Protoc. Immunol.* 123:e58. doi: 10.1002/cpim.58

Arstikaitis, P., Gauthier-Campbell, C., Carolina Gutierrez Herrera, R., Huang, K., Levinson, J. N., Murphy, T. H., et al. (2008). Paralemmin-1, a modulator of filopodia induction is required for spine maturation. *Mol. Biol. Cell* 19, 2026–2038. doi: 10.1091/mbc.e07-08-0802

Baines, A. J. (2010). The spectrin-ankyrin-4.1-adducin membrane skeleton: adapting eukaryotic cells to the demands of animal life. *Protoplasma* 244, 99–131. doi: 10.1007/s00709-010-0181-1

Baumert, R., Ji, H., Paulucci-Holthauzen, A., Wolfe, A., Sagum, C., Hodgson, L., et al. (2020). Novel phospho-switch function of delta-catenin in dendrite development. *J. Cell Biol.* 219:e201909166. doi: 10.1083/jcb.201909166

Bennett, V., and Lorenzo, D. N. (2016). An adaptable spectrin/ankyrin-based mechanism for long-range organization of plasma membranes in vertebrate tissues. *Curr. Top. Membr.* 77, 143–184. doi: 10.1016/bs.ctm.2015.10.001

Bodakuntla, S., Nedozralova, H., Basnet, N., and Mizuno, N. (2021). Cytoskeleton and membrane organization at axon branches. *Front. Cell Dev. Biol.* 9:707486. doi: 10.3389/fcell.2021.707486

Broderick, M. J., and Winder, S. J. (2005). Spectrin, alpha-actinin, and dystrophin. *Adv. Protein Chem.* 70, 203–246. doi: 10.1016/S0065-3233(05)70007-3

Dong, X., Shen, K., and Bulow, H. E. (2015). Intrinsic and extrinsic mechanisms of dendritic morphogenesis. *Annu. Rev. Physiol.* 77, 271–300. doi: 10.1146/annurev-physiol-021014-071746

Donta, M. S., Srivastava, Y., and McCrea, P. D. (2022). Delta-catenin as a modulator of rho GTPases in neurons. *Front. Cell. Neurosci.* 16:939143. doi: 10.3389/fncel.2022.939143

Donta, M. S., Srivastava, Y., Di Mauro, C. M., Paulucci-Holthauzen, A., Waxham, M. N., and McCrea, P. D. (2023). p120-catenin subfamily members have distinct as well as shared effects on dendrite morphology during neuron development in vitro. *Front. Cell. Neurosci.* 17:1151249. doi: 10.3389/fncel.2023.1151249

Fischer, T. D., Dash, P. K., Liu, J., and Waxham, M. N. (2018). Morphology of mitochondria in spatially restricted axons revealed by cryo-electron tomography. *PLoS Biol.* 16:e2006169. doi: 10.1371/journal.pbio.2006169

Fukata, Y., and Fukata, M. (2010). Protein palmitoylation in neuronal development and synaptic plasticity. *Nat. Rev. Neurosci.* 11, 161–175. doi: 10.1038/nrn2788

Gauthier-Campbell, C., Bredt, D. S., Murphy, T. H., and El-Husseini Ael, D. (2004). Regulation of dendritic branching and filopodia formation in hippocampal neurons by specific acylated protein motifs. *Mol. Biol. Cell* 15, 2205–2217. doi: 10.1091/mbc.e03-07-0493

Gireud-Goss, M., Reyes, S., Tewari, R., Patrizz, A., Howe, M. D., Kofler, J., et al. (2020). The ubiquitin ligase UBE4B regulates amyloid precursor protein ubiquitination, endosomal trafficking, and amyloid beta42 generation and secretion. *Mol. Cell. Neurosci.* 108:103542. doi: 10.1016/j.mcn.2020.103542

Gu, D., Sater, A. K., Ji, H., Cho, K., Clark, M., Stratton, S. A., et al. (2009). Xenopus delta-catenin is essential in early embryogenesis and is functionally linked to cadherins and small GTPases. *J. Cell Sci.* 122, 4049–4061. doi: 10.1242/jcs.031948

Herrick, S., Evers, D. M., Lee, J. Y., Udagawa, N., and Pak, D. T. (2010). Postsynaptic PDLIM5/enigma homolog binds SPAR and causes dendritic spine shrinkage. *Mol. Cell. Neurosci.* 43, 188–200. doi: 10.1016/j.mcn.2009.10.009

Horiuchi, Y., Arai, M., Niizato, K., Iritani, S., Noguchi, E., Ohtsuki, T., et al. (2006). A polymorphism in the PDLIM5 gene associated with gene expression and schizophrenia. *Biol. Psychiatry* 59, 434–439. doi: 10.1016/j.biopsych.2005.07.041

Horiuchi, Y., Ishikawa, M., Kaito, N., Iijima, Y., Tanabe, Y., Ishiguro, H., et al. (2013). Experimental evidence for the involvement of PDLIM5 in mood disorders in hetero knockout mice. *PLoS One* 8:e59320. doi: 10.1371/journal.pone.0059320

Hu, B., Copeland, N. G., Gilbert, D. J., Jenkins, N. A., and Kilimann, M. W. (2001). The paralemmin protein family: identification of paralemmin-2, an isoform differentially spliced to AKAP2/AKAP-KL, and of palmdelphin, a more distant cytosolic relative. *Biochem. Biophys. Res. Commun.* 285, 1369–1376. doi: 10.1006/bbrc. 2001.5329

Hultqvist, G., Ocampo Daza, D., Larhammar, D., and Kilimann, M. W. (2012). Evolution of the vertebrate paralemmin gene family: ancient origin of gene duplicates suggests distinct functions. *PLoS One* 7:e41850. doi: 10.1371/journal.pone.0041850

Kalebic, N., Gilardi, C., Stepien, B., Wilsch-Brauninger, M., Long, K. R., Namba, T., et al. (2019). Neocortical expansion due to increased proliferation of basal progenitors is linked to changes in their morphology. *Cell Stem Cell* 24, 535–550.e9. doi: 10.1016/j. stem.2019.02.017

Kato, T., Iwayama, Y., Kakiuchi, C., Iwamoto, K., Yamada, K., Minabe, Y., et al. (2005). Gene expression and association analyses of LIM (PDLIM5) in bipolar disorder and schizophrenia. *Mol. Psychiatry* 10, 1045–1055. doi: 10.1038/sj.mp.4001719

Kutzleb, C., Sanders, G., Yamamoto, R., Wang, X., Lichte, B., Petrasch-Parwez, E., et al. (1998). Paralemmin, a prenyl-palmitoyl-anchored phosphoprotein abundant in neurons and implicated in plasma membrane dynamics and cell process formation. *J. Cell Biol.* 143, 795–813. doi: 10.1083/jcb.143.3.795

Lanoue, V., and Cooper, H. M. (2019). Branching mechanisms shaping dendrite architecture. *Dev. Biol.* 451, 16–24. doi: 10.1016/j.ydbio.2018.12.005

Lasorella, A., and Iavarone, A. (2006). The protein ENH is a cytoplasmic sequestration factor for Id2 in normal and tumor cells from the nervous system. *Proc. Natl. Acad. Sci. U.S.A.* 103, 4976–4981. doi: 10.1073/pnas.0600168103

Lefebvre, J. L. (2021). Molecular mechanisms that mediate dendrite morphogenesis. *Curr. Top. Dev. Biol.* 142, 233–282. doi: 10.1016/bs.ctdb.2020.12.008

Li, C., Tao, R., Qin, W., Zheng, Y., He, G., Shi, Y., et al. (2008). Positive association between PDLIM5 and schizophrenia in the Chinese Han population. *Int. J. Neuropsychopharmacol.* 11, 27–34. doi: 10.1017/S1461145707007687

Li, X., Matsuoka, Y., and Bennett, V. (1998). Adducin preferentially recruits spectrin to the fast growing ends of actin filaments in a complex requiring the MARCKS-related domain and a newly defined oligomerization domain. *J. Biol. Chem.* 273, 19329–19338. doi: 10.1074/jbc.273.30.19329

Liu, Z., Liu, W., Xiao, Z., Wang, G., Yin, S., Zhu, F., et al. (2008). A major single nucleotide polymorphism of the PDLIM5 gene associated with recurrent major depressive disorder. *J. Psychiatry Neurosci.* 33, 43–46.

Ma, S., and Zuo, Y. (2022). Synaptic modifications in learning and memory - A dendritic spine story. *Semin. Cell Dev. Biol.* 125, 84–90. doi: 10.1016/j.semcdb.2021. 05.015

Martinez, M. C., Ochiishi, T., Majewski, M., and Kosik, K. S. (2003). Dual regulation of neuronal morphogenesis by a delta-catenin-cortactin complex and Rho. *J. Cell Biol.* 162, 99–111. doi: 10.1083/jcb.200211025

Nakagawa, N., Hoshijima, M., Oyasu, M., Saito, N., Tanizawa, K., and Kuroda, S. (2000). ENH, containing PDZ and LIM domains, heart/skeletal muscle-specific protein, associates with cytoskeletal proteins through the PDZ domain. *Biochem. Biophys. Res. Commun.* 272, 505–512. doi: 10.1006/bbrc.2000.2787

Naydenov, N. G., and Ivanov, A. I. (2011). Spectrin-adducin membrane skeleton: a missing link between epithelial junctions and the actin cytoskeleton? *Bioarchitecture* 1, 186–191. doi: 10.4161/bioa.1.4.17642

Popova, N. K., Ilchibaeva, T. V., and Naumenko, V. S. (2017). Neurotrophic factors (BDNF and GDNF) and the serotonergic system of the brain. *Biochemistry (Mosc)* 82, 308–317. doi: 10.1134/S0006297917030099

Portera-Cailliau, C., Pan, D. T., and Yuste, R. (2003). Activity-regulated dynamic behavior of early dendritic protrusions: evidence for different types of dendritic filopodia. *J. Neurosci.* 23, 7129–7142. doi: 10.1523/JNEUROSCI.23-18-07129. 2003

Puram, S. V., and Bonni, A. (2013). Cell-intrinsic drivers of dendrite morphogenesis. *Development* 140, 4657–4671. doi: 10.1242/dev.087676

Ren, B., Li, X., Zhang, J., Fan, J., Duan, J., and Chen, Y. (2015). PDLIM5 mediates PKCepsilon translocation in PMA-induced growth cone collapse. *Cell. Signal.* 27, 424–435. doi: 10.1016/j.cellsig.2014.12.005

Runge, K., Cardoso, C., and de Chevigny, A. (2020). Dendritic spine plasticity: function and mechanisms. *Front. Synaptic Neurosci.* 12:36. doi: 10.3389/fnsyn.2020. 00036

Rusakov, D. A., and Stewart, M. G. (2021). Synaptic environment and extrasynaptic glutamate signals: the quest continues. *Neuropharmacology* 195:108688. doi: 10.1016/ j.neuropharm.2021.108688

Thomas, D. G., and Robinson, D. N. (2017). The fifth sense: mechanosensory regulation of alpha-actinin-4 and its relevance for cancer metastasis. *Semin. Cell Dev. Biol.* 71, 68–74. doi: 10.1016/j.semcdb.2017.05.024

Valnegri, P., Puram, S. V., and Bonni, A. (2015). Regulation of dendrite morphogenesis by extrinsic cues. *Trends Neurosci.* 38, 439–447. doi: 10.1016/j.tins. 2015.05.003

Yan, Y., Tsukamoto, O., Nakano, A., Kato, H., Kioka, H., Ito, N., et al. (2015). Augmented AMPK activity inhibits cell migration by phosphorylating the novel substrate Pdlim5. *Nat. Commun.* 6:6137. doi: 10.1038/ncomms 7137

Zain, M. A., Roffeei, S. N., Zainal, N. Z., Kanagasundram, S., and Mohamed, Z. (2013). Nonsynonymous polymorphisms of the PDLIM5 gene association with the occurrence of both bipolar disorder and schizophrenia. *Psychiatr. Genet.* 23, 258–261. doi: 10.1097/YPG.0000000000000015

Zang, Y., Chaudhari, K., and Bashaw, G. J. (2021). New insights into the molecular mechanisms of axon guidance receptor regulation and signaling. *Curr. Top. Dev. Biol.* 142, 147–196. doi: 10.1016/bs.ctdb.2020.11.008